Eur. Phys. J. D **31**, 395–402 (2004)
DOI: 10.1140/epjd/e2004-00167-2

THE EUROPEAN PHYSICAL JOURNAL D

Laser-cooling molecules

Concept, candidates, and supporting hyperfine-resolved measurements of rotational lines in the A–X(0,0) band of CaH

M.D. Di Rosa[a]

Los Alamos National Laboratory, Mail Stop J567, Los Alamos NM 87545, USA

Received 16 August 2004
Published online 23 November 2004 –

Abstract. Certain molecules, it seems, may be laser cooled by methods technically similar to those applied with abundant success in atomic physics. We discuss the spectroscopic criteria molecules should meet to make methods of Doppler cooling technically feasible and identify diatomic candidates. Some candidates, such as the alkaline-earth monohydrides (e.g. BeH and CaH), are paramagnetic and amenable to magneto-optical trapping. Our experimental study concentrates on CaH, and we present our recent high-resolution, molecular-beam-based measurements of low-J rotational lines within the $A-X(0,0)$ band of CaH. From these measurements we report hyperfine separations in the A-state, as important to laser-cooling spectroscopy, and centroidal transition frequencies for comparison with existing values. We conclude with an outline of a possible magneto-optical trap for CaH.

PACS. 33.80.Ps Optical cooling of molecules; trapping – 33.70.Fd Absolute and relative line and band intensities – 33.15.Pw Fine and hyperfine structure

1 Introduction

The ITAMP Workshop on Ultracold Polar Molecules: Formation and Collisions held 8-10 January 2004 bore witness to the diverse approaches in cooling molecules and their rapid progress. We introduce here the possibility of extending the successful approach in atomic physics of laser cooling through repeated cycles of absorption and spontaneous emission to certain molecules. In doing so, we trade the generality of the laser-cooling scheme outlined by Bahns et al. [1] for one of restricted applicability but built from known and comparatively simpler technologies. Thus while not a general approach, the method described here might prove a feasible way of cooling select molecules to sub-millikelvin translational temperatures in the lowest rovibrational level of their ground electronic state. A MOT-like dissipative trap in itself is conceivable, or one could add the hallmark of laser cooling of phase-space compression to an otherwise conservative-force trap or decelerator [2,3] (with note that conservative forces cannot increase the phase-space density of an ensemble, methods of stochastic cooling excepted [4]). Owing to molecular structure, laser cooling as presented here through cycles of electronic transitions cannot be as efficient as for atoms. But perfect efficiency, where particles are never lost from the cooling cycle, is not necessary to reap the benefits of laser cooling. Techniques of Doppler cooling, for example, can increase the phase-space density of an atomic beam by factors of $>10^6$ [5] and so can admit fairly low efficiencies while still providing significant gains in phase-space density. We list later in Table 1 a collection of molecules which, on application of a modest technical complexity beyond that used for laser cooling atoms, can undergo $\geq 1\times10^4$ cycles of absorption and emission through allowed electronic transitions with efficiencies on the order of 1–10%. For such molecules laser cooling then becomes, along with the demonstrated method of buffer-gas cooling [6] and possible adaptations of stochastic cooling [4,7], a way of increasing the phase-space density of a molecular ensemble before recourse to evaporative cooling and reliance on favorable rates of elastic self-collisions.

1.1 Laser-cooling criteria

As with atomic systems, molecules must meet certain criteria to be considered candidates for laser cooling. Briefly, these criteria include (1) a band system with strong (i.e. large oscillator strength) one-photon transitions to ensure the high photon-scattering rates needed for rapid laser cooling, (2) a highly-diagonal Franck-Condon array for the band system, and (3) no intervening electronic states to which the upper state could radiate and terminate the cycling transition. The second criterion acknowledges the convenience if not the practical necessity of limiting the

[a] e-mail: mdd@lanl.gov

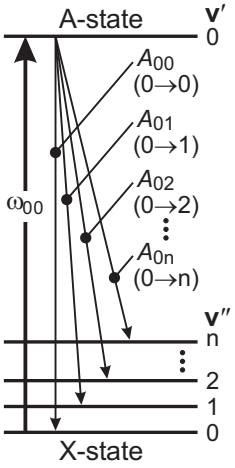

Fig. 1. Fluorescence cascade within a generic electronic band system following the vibronic excitation $v'' = 0 \leftarrow v' = 0$.

number of lasers required to keep the molecule in a closed-loop cooling cycle. This point is emphasized through the simple vibronic-structure diagram of Figure 1, which depicts the fluorescence (spontaneous emission) cascade of an electronic-band system following excitation from the zeroth vibrational level ($v'' = 0$) of the ground electronic state (X) to the zeroth vibrational level ($v' = 0$) of an electronically-excited state (A). The probability for fluorescence decay from $v' = 0$ to $v = 0$, 1, and 2 is in proportion to the band spontaneous-emission rates of A_{00}, A_{01}, and A_{02}, respectively. So-called diagonal systems have $A_{00} \gg A_{01} \gg A_{02} \gg A_{03}\ldots$, meaning that the ground-state disposition following radiative decay from $v' = 0$ is heavily weighted toward $v'' = 0$, with populations in higher vibrational levels vanishing quickly with v''. A closed-loop absorption/emission cycle is then formed by pumping transitions along $A(v = 0) \leftarrow X(v = 0)$ and then along $A(v = 0) \leftarrow X(v > 0)$ as necessary to limit the inefficiency, or loss of molecules, in the cooling cycle.

The repeated cycles of absorption and emission describe a Bernoulli sequence, and we assign p as the probability the molecule will not absorb a photon to begin any one cycle because it has been placed by spontaneous emission in a ground state outside those covered by the cooling cycle. Essentially, p is the ratio of the fluorescence rate to vibrational levels outside the range of cooling/repump transitions to the total fluorescence rate. The probability P that a molecule will undergo a sequence of N cooling cycles is then $(1-p)^N$. When considering a collection of molecules, we interpret P to give the fraction of molecules remaining through N absorption/emission cycles, and $(1 - P)$ the fraction of molecules lost.

Individual cases, of course, will dictate the acceptable percentage of molecules that may be lost irretrievably from the cooling cycle, and we offer the following example of Doppler cooling for consideration. A representative molecule, perhaps jetted from the pulsed molecular microbeam of Zhao et al. [8], has a terminal velocity of $V = 100$ m/s, a molecular weight of $m = 30$ amu, and a nearly diagonal $A{-}X$ system with absorption and emission along $A{-}X(0,0)$ at nominally $\lambda = 600$ nm. We wish to slow within a reasonable distance at least 10% of the molecules (those that have an initial quantum state suitable for entering the cooling cycle) to a halt, a feat that requires our molecule to undergo $mV\lambda/h = 4500$ absorption/emission events. For ten percent or more ($P \geq 0.10$) of the molecules to sustain 4500 such Bernoulli trials ($N = 4500$), the probability of spontaneous emission to v'' outside those encompassed by the cooling cycle must be $\leq$0.05% (or $p \leq 5 \times 10^{-4}$). As it turns out, molecular systems for which $\geq$99.95% of the spontaneous emission from $v' = 0$ is confined to vibronic branches $v' = 0 \rightarrow v'' = 0$ and $0{\rightarrow}1$ are not so rare. Assuming it had the typical upper-state lifetime of 100 ns, our representative molecule could be brought from 100 m/s to rest within 5–10 cm.

1.2 Candidate molecules

Molecules and their associated band systems that reasonably meet the aforementioned criteria are listed in Table 1. The emission probability A_{00} and nominal wavelength, λ_{00}, of the $0{\rightarrow}0$ band are given for estimating the maximum possible scattering rate and scattering force through $A_{00}/2$ and $hA_{00}/2\lambda_{00}$, respectively. The nominal wavelength, λ_{01} [nm], of the 0–1 band is also listed. The probability for emission to $v'' = 1$ and $v'' = 2$ is given relative to A_{00} by ratios A_{01}/A_{00} and A_{02}/A_{00}, respectively. Values are from measurements or theoretical calculations or both, or otherwise omitted when neither was available. References pertinent to an entry are listed in square brackets. The A_{00}, if not reported explicitly, were based on either the upper-state ($v' = 0$) lifetime or the $0{\leftarrow}0$ absorption oscillator strength as multiplied by an exact conversion factor [31]. Ratios A_{01}/A_{00} and A_{02}/A_{00}, if not explicitly available, were based on (appropriately weighted [31]) ratios of absorption oscillator strengths or Franck-Condon factors; the first basis provides the emission-probability ratio exactly while the latter yields a reasonable estimate to the extent the transition dipole moment varies little with internuclear separation. For the $\Pi - \Sigma$ bands of Table 1, magnetic dipole transitions (wherein transitions of $\Delta J = 0, \pm 1$ terminate on states of the "wrong" parity) occur at a rate of 1 transition or less in 10^5 [32] and would also require attention when forming a highly-closed cooling cycle.

Table 1 is not intended to be a comprehensive list of candidate molecules for laser cooling. Absent, for example, are tri- and polyatomics. The technique would seem to be a technical challenge already for diatomics, and polyatomics present the further complexity of having to "track" in a pump/repump scheme additional vibrational coordinates beyond the one of a diatomic. Among other possible diatomic candidates are isotopic variants of those listed in Table 1 (the fermionic $^{40}Ca^{2}H$ instead of bosonic $^{40}Ca^{1}H$) and the alkaline-earth monohalides (e.g., the $A{-}X$ band of CaCl [33]). In cases where very low scattering rates are suitable, one may also consider cooling the lead monohalides, particularly PbCl, through their (magnetic dipole) fine-structure transitions

Table 1. Diagonal molecular band systems as candidates for laser cooling.

Molecule	Band	λ_{00} [nm]	λ_{01}[nm]	$A_{00} \times 10^{-6}$ [s^{-1}]	$(A_{01}/A_{00}) \times 10^3$	$(A_{02}/A_{00}) \times 10^4$
BeH	$A^2\Pi_r - X^2\Sigma^+$	499.2 [9]	554.2 [9]	12.3−15.3 [10, 11]	5.4−6.0 [10, 11]	0.75−5.8 [10, 11]
MgH	$A^2\Pi_r - X^2\Sigma^+$	518.7 [12]	562.3 [12]	23.3–40.0 [10, 13]	46−55 [10, 13]	24−35 [10, 13]
CaH	$A^2\Pi_r - X^2\Sigma^+$	693.0 [14]	759.3 [14]	14.3 [15, 16]	12−17 [15−18]	0.7−3 [15−18]
SrH	$A^2\Pi_r - X^2\Sigma^+$	739.4 [19]	815.0 [19]	29.6 [20]	15 [20]	—
BaH	$A^2\Pi_r - X^2\Sigma^+$	1034 [12]	1176 [12]	—	3.9 [18]	0.5 [18]
NH	$A^3\Pi_i - X^3\Sigma^-$	335.8 [12]	377.4 [12]	2.26 [21]	6–7 [22, 23]	1.8 [24]
BH	$A^1\Pi - X^1\Sigma^+$	433.2 [25]	482.6 [25]	7.8 [26]	5 [26]	—
AlH	$A^1\Pi - X^1\Sigma^+$	424.1 [27]	457.6 [27]	15 [28]	1.8 [27]	—
AlF	$A^1\Pi - X^1\Sigma^+$	227.5 [12]	231.8 [12]	529.3 [29]	<0.1 [29]	<0.1 [29]
AlCl	$A^1\Pi - X^1\Sigma^+$	261.5 [12]	264.9 [12]	160−190 [29, 30]	<0.1 [29]	<0.1 [29]

($^2\Pi_{3/2}$−$^2\Pi_{1/2}$) in the near infrared, or cooling heteronuclear diatomics through rovibrational transitions in the near- to mid-infrared.

Experimental convenience aside, the aluminum monohalides appear very well suited for laser cooling with large A_{00} (thus high scattering rates) and very low scattering probabilities into off-diagonal bands 0→1 and 0→2. However, among the candidate molecules of Table 1, we chose to study CaH first because techniques for generating CaH are known, commercial equipment can provide the needed cw laser wavelengths and power, and spectroscopic information for this molecule of astrophysical importance has become abundant since its "discovery" in 1908 when Olmsted concluded that a "compound of calcium and hydrogen" within his calcium-arc discharge was emitting bands of light coincident with those from sun spots [34]. The measurements of the A−X(0,0) band presented here complement the CaH literature with improved precision for line positions and hitherto unavailable hyperfine separations in the A-state, as integral to the laser-cooling cycle.

2 Example laser-cooling cycle for CaH

Cooling cycles for the $A^2\Pi_r$−$X^2\Sigma^+$ system of CaH, wherein the $^2\Pi$ state approximates an angular momentum coupling of Hund's case (a), can be based on transitions to either of the two upper-state spin-orbit components $A^2\Pi_{1/2}$ or $A^2\Pi_{3/2}$. Figure 2 shows a pair of allowed transitions, designated by bold arrows, that effect a main cooling cycle in connection with $A^2\Pi_{1/2}$. Hyperfine structure is omitted from the figure for diagrammatic clarity and will be introduced later. The two transitions, labeled (0,0)$Q_1(0.5)$ and (0,0)$P_{12}(1.5)$ by spectroscopic convention [35], incorporate the lowest energy state of CaH of $X^2\Sigma^+(v = 0,\ N = 0,\ J = 0.5)$ and share the same upper state of $A^2\Pi_{1/2}(v = 0,\ J = 0.5,\ p^-)$. Such a Λ-type transition configuration has been used successfully to trap atoms (along the D_1 line [36]) and to rectify the optical dipole force for cooling, accelerating, or deflecting atomic beams [37]. Dashed arrows indicate the pair of repump transitions [(0,1)$Q_1(0.5)$ and (0,1)$P_{12}(1.5)$] that return rotational populations of $J'' = 0.5$ and 1.5 in $v'' = 1$, as occupied once or twice every 100 events of spontaneous emission from $v' = 0$ (see A_{01}/A_{00} in Tab. 1), back to the main cooling cycle. With light stimulating the main (0←0) and repump (0←1) transitions, the cooling cycle becomes closed except for about one absorption event in 10^4 owing to chance spontaneous emission from $v' = 0$ to $v'' = 2$ (see A_{02}/A_{00} in Tab. 1). The presence of interference transitions, the thin arrows in Figure 2, can also influence the degree to which the cooling cycle is closed. Interference transitions have frequencies close to that of the main and repump light and stem from the same ground states as the main and repump transitions. Their connection, however, with upper

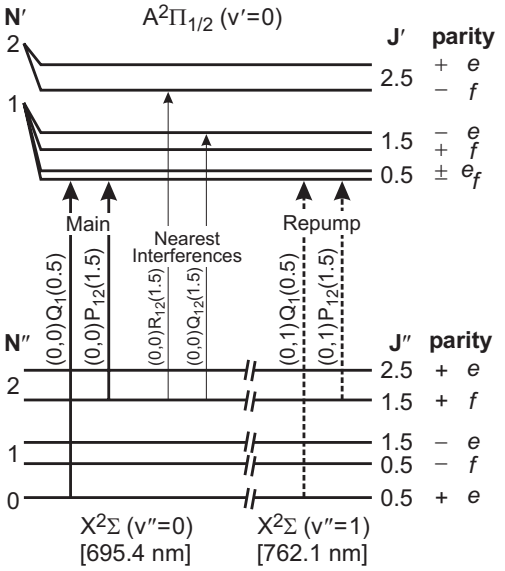

Fig. 2. Energy diagram (not to scale) showing one of several cooling cycles possible for CaH, this one connecting $X^2\Sigma^+$ and $A^2\Pi_{1/2}$ and incorporating the lowest internal-energy state of $N'' = 0$, $J'' = 0.5$. The pair of main (bold line) and repump (dashed line) transitions of the cooling cycle stem from $v'' = 0$ and $v'' = 1$, respectively, and terminate at the same upper state in $v' = 0$. From Table 1, the pairs of main and repump transitions afford a cooling cycle that is closed to about 1 absorption event in 10^4, owing to loss by spontaneous emission to $v'' = 2$. The nearest interference transitions, indicated by dashed lines, are sufficiently distant from the main/repump pairs to cause little concern of spoiling the degree of cooling-cycle closure (see text). Values in square brackets refer to the average wavelengths of the associated main and repump transitions. The e/f parity assignments follow the recommendation of Brown et al. [J. Mol. Spectrosc. **55**, 500 (1975)].

states different from those of the main and repump transitions leads to molecular loss from the cooling cycle, as spontaneous emission following their excitation populates ground-state levels outside those covered by the cooling cycle. In the case described here for CaH, and based on spectroscopic constants from Berg and Klynning [14], $(0,0)R_{12}(1.5)$ presents the closest interference at a separation of $\delta = 6.2$ cm^{-1} from $(0,0)Q_1(0.5)$, a separation of 1.7×10^5 times the half-width-at-half-maximum natural width ($\Delta\nu_n$) of the $A - X$ transitions of CaH of 1.1 MHz. Because $\delta \gg \Delta\nu_n$, the probability of exciting the interference transition over $(0,0)Q_1(0.5)$ scales as $(\Delta\nu_n/\delta)^2 \sim 3 \times 10^{-11}$, which is insignificant compared with the other probabilities in this case (e.g., A_{02}/A_{00}) that limit the cooling-cycle efficiency. The repump transitions are similarly well isolated. The values 695.4 nm and 762.1 nm in square brackets at the bottom of Figure 2 give the average wavelengths of the main and repump transitions, respectively. Calculated [14] frequencies in units of cm^{-1} for the main and repump transitions are: $(0,0)Q_1(0.5)/14393.63$, $(0,0)P_{12}(1.5)/14368.19$, $(0,1)Q_1(0.5)/13133.44$, $(0,1)P_{12}(1.5)/13108.72$.

3 Measured hyperfine structure of CaH A–X rotational lines

Knowledge of hyperfine structure, when present, is essential to the success of a laser-cooling scheme. For the common isotope ^{40}Ca^{1}H (designated simply CaH henceforth) each rotational state (J) of the ground ($X^2\Sigma^+$) and upper ($A^2\Pi_r$) electronic state harbors a twofold nuclear-spin degeneracy that is split on the order of 1–100 MHz by mainly the hyperfine interaction of the electron spin with the spin-1/2 hydrogen nucleus. We assume the $X^2\Sigma^+$ and $A^2\Pi_r$ states of CaH have hyperfine coupling cases [38,39] (for zero and weak external fields) of $(b)_{\beta J}$ and $(a)_\beta$, respectively, which lets us form in both states the total angular momentum F from $J + I$, where the nuclear spin $I = 1/2$ for CaH. The rotational level $J = 0.5$ is thus split into total angular momentum states $F = 0$ and 1, $J = 1.5$ divides to $F = 1$ and 2, and so on. Because hyperfine splittings are known (for low J) for the X-state [40,41], high-resolution measurements of $A-X$ rotational lines may then be used to extract hyperfine splits in the A-state, which are thus far unknown.

3.1 Rotational-line hyperfine structure

The P, Q, and R rotational lines within the $A-X$ band of CaH comprise 3 or 4 hyperfine transitions, as dictated by the usual selection rules of $\Delta F = 0$ and ±1 but $0\not\leftrightarrow0$. The intensities of hyperfine transitions within a rotational line may be compared through the appropriate 6-j coefficients [42] when, as is the case in our experiment, the thermal energy greatly exceeds the ground-state hyperfine separation. In Figure 3, lines $Q_1(0.5)$ and $P_{12}(2.5)$ are shown separated into their constituent hyperfine transitions. Parenthetical values give the expected relative intensities of the hyperfine transitions within the rotational line. The separation and ordering of hyperfine-level pairs for the X-state rotational levels of Figure 3 is from the microwave measurements of Barclay et al. [40] and Frum et al. [41]. Hyperfine separations are expected in the upper state as well, and in Figure 3 the symbols δ_{10} and δ_{21} are placeholders for the anticipated energy difference between $F' = 1$ and $F' = 0$ of $|J' = 0.5,\ \Omega = 1/2,\ p^-\rangle$ and between $F' = 2$ and $F' = 1$ of $|J' = 1.5,\ \Omega = 1/2,\ p^+\rangle$, respectively. The hyperfine splits δ_{10} and δ_{21} were then extracted from our high-resolution measurements of $Q_1(0.5)$ and $P_{12}(2.5)$, obtained in the following manner.

3.2 Description of experiment

Our molecular-beam machine comprises a source chamber (where CaH is generated continuously and issues in a jet) followed by three differentially-pumped chambers separated by skimmers. An oven within the source chamber reacts Ca(g) + H_2 in an Ar buffer at ∼1300 K and ∼100 Torr to form several mTorr of CaH, which, along with the total mixture, is jetted, adiabatically cooled to

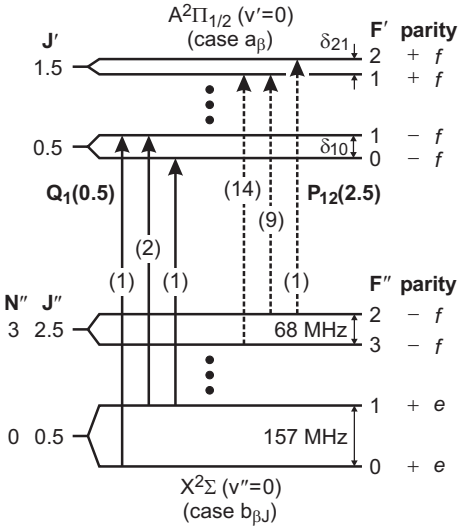

Fig. 3. Hyperfine composition of (some) low-J rotational lines within the $A-X(0,0)$ band of CaH. Arrows within the energy diagram (not drawn to scale) show the hyperfine structure underlying rotational lines $(0,0)Q_1(0.5)$ (solid arrows) and $(0,0)P_{12}(2.5)$ (dashed arrows). The relative strength of a hyperfine transition within its parent rotational line is given by a parenthetical value. The hyperfine separations in $v'' = 0$ are from references [40,41]. The hyperfine separations indicated in $v' = 0$ were measured here to be $\delta_{10} = 17\pm1$ MHz and $\delta_{21} = 1\pm1$ MHz.

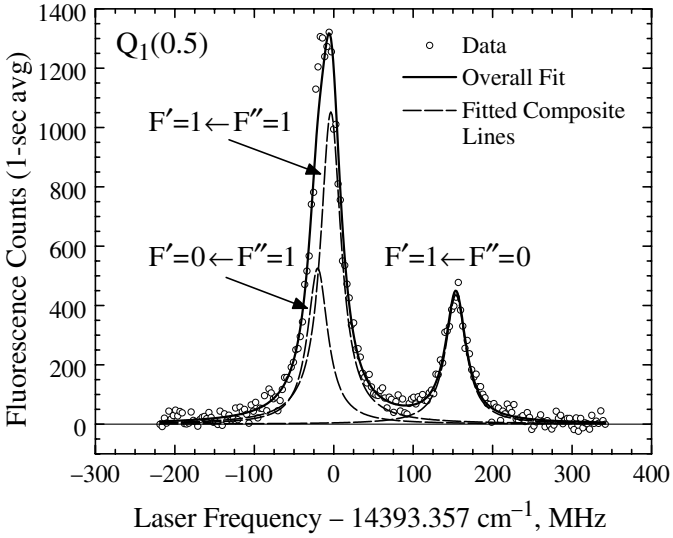

Fig. 4. Rotational line $Q_1(0.5)$ within the $A-X(0,0)$ band of CaH measured in laser-induced fluorescence from a continuous molecular beam. The cw laser beam was linearly polarized orthogonal to the fluorescence-collection axis and had an irradiance of ∼500 mW/cm^2. The measured profile was fitted to three equal-width Lorentzian profiles (dashed lines), representing the constituent hyperfine transitions (see Fig. 3). The relative areas (heights) of the profiles are close to theoretical expectations. A best-fit separation of 17±1 MHz between the profiles representing transitions 1←1 and 0←1 gave the upper-state hyperfine separation δ_{10} of Figure 3.

∼200 K, and collimated by skimmers on approach to the final diagnostics chamber, where at a distance of 1.3 m from the jet orifice the estimated flux of CaH is 5×10^7 cm^{-2} s^{-1} per quantum state (at low J''). The diagnostics chamber is equipped with a quadrupole mass spectrometer and the optical ports necessary for measuring the rotational lines of CaH through laser-induced fluorescence (LIF). The molecular beam, a cw laser beam, and the fluorescence-collection axis intersect at mutually orthogonal angles at the center of the diagnostics chamber. A red-sensitive and cooled (to –30 °C) photomultiplier tube (PMT) measures the essentially resonant fluorescence of CaH induced by laser excitation of $A\leftarrow X(0,0)$ transitions. A single lens collects the LIF with $f/2$ efficiency and focuses the fluorescence onto a ∅1 mm field stop at the PMT.

The cw laser is a commercial ring dye laser operating with LD 688 laser dye (from Exciton) at a concentration of 0.5 g in 1 liter of 2-phenoxyethanol and pumped with 5 W of 532 nm light from a cw Nd:YVO4 laser. The dye laser is actively stabilized and has a line width of ∼1 MHz. At the probe volume, located at the center of the diagnostics chamber, the laser power is steady and typically 1 to 3 mW, the beam waist is about 0.5 mm, and the laser polarization is linear and aligned orthogonal to the axis of fluorescence collection.

The low fluorescence signal warrants the use of photon-counting techniques and electronics. Peak photoelectron count rates are typically $1-2\times10^3$ s^{-1} and occur when the laser frequency coincides with resonances of the low-J'' absorption features recorded here. The background signal from laser scatter (off walls and surfaces) was diminished to 10% or less of the peak count rate through the use of light baffles and optically-black chamber surfaces.

Spectra are recorded under computer control. The laser frequency is stepped in increments of ∼3 MHz and is paused between steps to collect and record the number of PMT counts for a particular duration (typically 1 s). The laser frequency at each pause is recorded as measured by a commercial wavemeter (a Burleigh/Exfo WA-1500).

3.3 Example measurement and analysis

A laser power of 1 mW, a fluorescence counting interval of 1 s, and a steady sequence of ∼3MHz steps in laser frequency produced the measured trace of $Q_1(0.5)$ shown in Figure 4. The frequency axis was linearized and placed on an absolute scale by the recorded sequence of wavemeter readings. The roughly 30 MHz width (FWHM) of the features is consistent with power-broadened widths owing to the laser-beam irradiance of 500 mW/cm^2. The two prominent features were fitted by least-squares minimization to three equal-width Lorentzian profiles (dashed lines), representing the three hyperfine transitions — $F' = 0 \leftarrow F'' = 1$, $F' = 1 \leftarrow F'' = 1$, and $F' = 1 \leftarrow F'' = 0$ — composing $Q_1(0.5)$. The fitting process was additionally constrained by a fixed separation between transitions 1←0 and 1←1 at the known ground-state hyperfine splitting of 157 MHz (refer to Fig. 3). The remaining variables

Table 2. Measured transition frequencies in the A–$X(0,0)$ band of CaH.

Line	Measured frequency [cm^{-1}]		
	This work*	Berg and Klynning [14]	Pereira et al. [44]
$P_{12}(2.5)$	14354.555(4)	14354.54	14356.57
$P_1(1.5)$	14385.830(4)	14385.83	14387.66
$Q_1(0.5)$	14393.359(4)	—	14395.36
$P_2(2.5)$	14428.475(4)	14428.44	14430.48
$Q_2(1.5)$	14453.873(4)	14453.88	14455.76

*Centroidal frequencies are given. Parenthetical value is the uncertainty (plus or minus) of the last digit.

in the fit were the center frequencies of the Lorentzian profiles, their shared width, and their areas (as proportional to the line strength). The best-fit separation between 1←1 and 0←1 yielded an upper-state hyperfine split of $\delta_{10} = 17 \pm 1$ MHz. A visual inspection of peak heights among the (equal width) constituent Lorentzians shows the fitted areas to have relative proportions in close agreement with the theoretical line-strength ratios of Figure 4. A second measurement of $Q_1(0.5)$ gave identical results. The rotational line $P_{12}(2.5)$ was similarly measured twice and yielded at our present resolution a barely discernible upper-state hyperfine split of $\delta_{21} = 1 \pm 1$ MHz.

3.4 Centroid-frequency comparison

Measurements of the $A-X(0,0)$ band of CaH succeeding the first systematic study by Hulthèn [43] in 1927 are provided by Berg and Klynning [14] and by Pereira and coworkers [44]. A new study of the $A-X$ and $B-X$ band systems of CaH by Steimle's group at Arizona State University will soon be published [45]. To this collection we add our hyperfine-resolved measurements of several rotational lines in the $A-X(0,0)$ band, performed in the manner described for $Q_1(0.5)$. Our measured frequencies of rotational lines are listed in Table 2 as the mean, centroidal frequency of the hyperfine-resolved line. Each reported frequency was determined from the average of two to four measurements of a rotational line. No dependence of centroidal frequency on laser power ranging from 0.7 to 3 mW was observed; ac Stark shifts were thus indiscernible at the laser irradiances used. Our uncertainty of ± 0.004 cm^{-1} combines the manufacturer-specified accuracy of the wavemeter ($\pm 2.9 \times 10^{-3}$ cm^{-1} at 695 nm) and allowance for a Doppler shift (proportional to $\vec{k} \cdot \vec{v}$) of $\pm 1.7 \times 10^{-3}$ cm^{-1} stemming from a possible $\pm 2^\circ$ deviation from perfect orthogonality between the laser wavevector ($\vec{k}$) and the velocity vector ($\vec{v}$) of the molecular beam. Included in Table 2 for comparison are measured values from the two most recently published studies of CaH line frequencies. Overall, our measurements offer an improved accuracy over those reported earlier and agree well with those of Berg and Klynning [14] and also the vintage work of Hulthèn [43], who could only give single frequencies for main/satellite pairs because of instrument-resolution blending (e.g. denoting $P_1(2.5) + Q_{12}(1.5)$ as $P_1(N'' = 2)$ at 14385.88 cm^{-1}). When corrected for what seems to be mistyped line labels, the measurements of Pereira et al. [44] appear to be displaced $\sim$1.9 cm^{-1} from our and others measurements.

4 Trapping spectroscopy

Owing to the paramagnetic property of its ground electronic state, CaH can be confined at low temperatures to a purely magnetic trap, as demonstrated by Doyle's group at Harvard [46,47]. By this same property, CaH can conceivably be captured by and cooled within a magneto-optical trap (MOT) [48] fashioned after those used routinely to trap alkali atoms. Figure 5 shows the energy-level diagram for trapping in one dimension along $F' = 0 \leftarrow F'' = 1$ of the $Q_1(0.5)$ transition shown in Figure 4. The diagram applies to $Q_1(0.5)$ in either the set of main or repump transitions (see Fig. 2). Along an axis (z) of the usual spherical magnetic quadrupole used in a MOT, the weak (from zero to tens of Gauss) magnetic field of form $B(z) = bz$ shifts a Zeeman sublevel $m_{F''}$ within the $X^2\Sigma^+$ ground state by energy $\Delta E''(z)$ [MHz] according to [39]

$$\Delta E''(z) \approx \mu_0 \, g_J \, B(z) \, m_{F''} \times \left[\frac{F\,(F+1) + J\,(J+1) - I\,(I+1)}{2F\,(F+1)} \right] \text{ [MHz]},$$

where $\mu_0 = 1.4$ MHz/G is the Bohr magneton, $I = 1/2$, B is in units of Gauss, and g_J is a molecular g factor particular to the electronic and rotational state and is of order unity [49,50]. The upper state $A^2\Pi_{1/2}(J' = 0.5)$ is essentially diamagnetic for our purposes [49,51], and the transitions nonetheless terminate on the magnetically unresponsive $F' = 0$ of $J' = 0.5$.

To produce the signature optical molasses and restoring force of a MOT, light tuned slightly below resonance from the three transitions of $\Delta m_F = 0, \pm 1$ connecting $F' = 0 \leftarrow F'' = 1$ is needed. Along an axis of the MOT, three co-propagating beams of distinct frequency and polarization stimulate the three Zeeman-sublevel transitions. The three beams shown directed from right-to-left along the z-axis of Figure 5 are distinguished by the frequency labels ω_0, ω_0+, and ω_0-. The same beams retrace the z-axis in the opposite direction, by retroreflection for example. Frequency ω_0 is nearly resonant with the $\Delta m_F = 0$

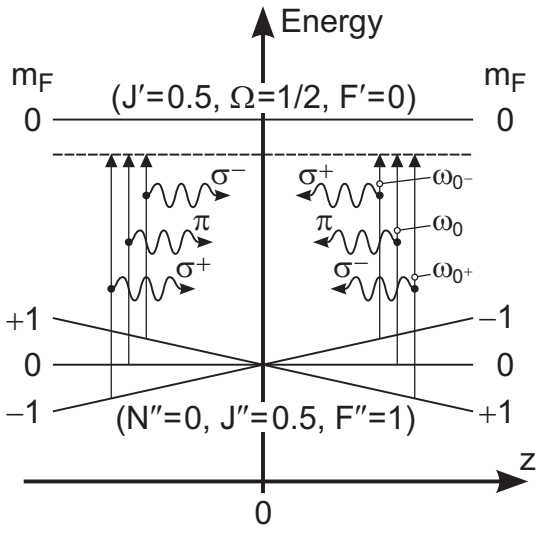

Fig. 5. Energy-level diagram (in 1-D) of a proposed MOT for CaH as produced through excitation of the hyperfine transition $F' = 0 \leftarrow F'' = 1$, a constituent transition of both $Q_1(0.5)$ and $P_{12}(1.5)$. The Zeeman response of the upper and lower states along an axis of the quadrupole field of a MOT is shown; the indicated laser frequencies, beam directions, and polarizations (σ for circular, π for linear) are arranged to produce the signature damping and restoring forces of a MOT. Signs for the magnetic hyperfine levels ($m_F = \pm 1$) and circular polarizations ($\sigma^{\pm}$) are referenced to the space-fixed axis.

transition while frequencies $\omega_0+ > \omega_0$ and $\omega_0- < \omega_0$ drive transitions of $\Delta m_F \neq 0$. The beams of frequency ω_0+ and ω_0- are both circularly polarized but with opposite senses, as indicated in Figure 5. When propagating in the $\pm z$-direction, the beam with frequency ω_0+ (ω_0-) has circular polarization $\sigma^{\pm}$ ($\sigma^{\mp}$) to drive $\Delta m_F = \pm 1$ ($\Delta m_F = \mp 1$) transitions (the directions, or signs, of σ and $m_{F''}$ in Figure 5 are referenced to the $+z$-axis). The beam with frequency ω_0 is linearly (π) polarized, provides no restoring force, but contributes to an optical-molasses-like friction and is essential for pumping the ground-state population out of $F'' = 0$, $m_{F''} = 0$. By this arrangement in total, the scattering force on the molecule has a net direction toward $z = 0$ for all the $m_{F''}$ populated by radiative decay from $F' = 0$ to $F'' = 1$. A diagram similar to Figure 5 can be sketched for trapping along $F' = 0 \leftarrow F'' = 1$ of $P_{12}(1.5)$. The MOT would of course require main and repump light along both $Q_1(0.5)$ and $P_{12}(1.5)$, as emphasized in Figure 3. Once molecules are trapped, the ensemble may be optically pumped into $v'' = 0$, $J'' = 0.5$ — the lowest internal energy state — by leaving on all light except that exciting $(0,0)Q_1(0.5)$.

The lifetime ($\tau_{1/e}$) of molecules within the MOT is limited by the extent of repump light along non-diagonal bands. In the case described here for CaH where repump light is provided along the (0,1) band, $\tau_{1/e}$ is $\leq$1 ms, a time sufficient to measure the presence of each captured molecule through its scattering of $\sim 10^4$ photons. The MOT would thus fluoresce brightly for as long as molecules were supplied. To the extent that analogies with atomic MOTs are permissible, we might anticipate loading rates (R [s^{-1}]) of a room-temperature molecular vapor into a MOT to be $R \approx 40nf$ [52], where the numerical factor is a rate constant [cm^3 s^{-1}], n [cm^{-3}] is the total density of molecules, and f is the fraction of molecules in quantum states connected to the cooling cycle. For the specific case of CaH, $f = 0.05$ assuming Boltzmann equilibrium at 300 K. Thus, were a density of CaH of $n \sim 10^8$ cm^{-3} (a pressure of 10^{-9} Torr) maintained in and equilibrated to a cell at 300 K, one could expect to see a bright and steady MOT holding on average $R\tau_{1/e} \sim 10^5$ molecules (neglecting the collision loss of molecules during their 1 ms stay in the trap). Lower cell-wall temperatures would increase f and also the rate constant for loading molecules into the MOT [53], the latter increase owing to an increased fraction of molecules having a velocity equal to or less than the capture velocity of the MOT (of typically 10–30 m/s for an atomic MOT [54]). The storage of molecules for periods longer and in numbers greater than possible by the MOT could be accomplished by multiple transfers of the MOT-captured ensembles into a spatially separate optical dipole trap, as demonstrated with atoms in a novel procedure by Davies et al. [55].

5 Conclusions

Diatomic molecules that meet certain criteria for laser cooling, such as possessing a strong and highly diagonal band system, are not all that rare. Among those candidates are also paramagnetic molecules, such as CaH, the focus of our experimental study, that seem suitable for magneto-optical trapping. As might be the case for other candidate molecules, we found the spectroscopic literature on CaH to be abundant but understandably lacking in some details important to laser cooling. Our molecular-beam machine was thus built to help complement the literature with the needed precision measurements, as reported here, and will later be configured to test our concepts in laser cooling.

The author is grateful for the technical assistance and equipment freely lent to the experiments by Johnny Anderson, Steven Buelow, Jeanne Robinson, Robert Sander, and David Viera of Los Alamos National Laboratory. This work is supported the Laboratory Directed Research and Development Program at Los Alamos National Laboratory, with supplemental funding from the Office of Nonproliferation Research and Engineering of the National Nuclear Security Administration.

References

1. J.T. Bahns, W.C. Stwalley, P.L. Gould, J. Chem. Phys. **104**, 9689 (1996)
2. H.L. Bethlem, F.M.H. Crompvoets, R.T. Jongma, S.Y.T. van de Meerakker, G. Meijer, Phys. Rev. A. **65**, 053416 (2002)
3. H. Nishimura, G. Lambertson, J.G. Kalnis, H. Gould, Rev. Sci. Instrum. **74**, 3271 (2003)

4. M.G. Raizen, J. Koga, B. Sundaram, Y. Kishimoto, H. Takuma, T. Tajima, Phys. Rev. A. **58**, 4757 (1998)
5. H.J. Metcalf, P. van der Straten, J. Opt. Soc. Am. B **20**, 887 (2003)
6. R. deCarvalho, J.M. Doyle, B. Freidrich, T. Guillet, J. Kim, D. Patterson, J.D. Weinstein, Eur. Phys. J. D **7**, 289 (1999)
7. F.M.H. Crompvoets, H.L. Bethlem, J. Küpper, A.J.A. van Roij, G. Meijer, Phys. Rev. A. **69**, 063406 (2004)
8. B.S. Zhao, M. Castillejo, D.S. Chung, B. Friedrich, Rev. Sci. Instr. **75**, 146 (2004)
9. C. Focsa, S. Firth, P.F. Bernath, R. Colin, J. Chem. Phys. **109**, 5795 (1998)
10. H.E. Popkie, J. Chem. Phys. **54**, 4597 (1971)
11. F.B.C. Machado, O. Roberto-Neto, F.R. Ornellas, Chem. Phys. Lett. **305**, 156 (1999)
12. K.P. Huber, G. Herzberg, *Molecular Spectra and Molecular Structure IV. Constants of Diatomic Molecules* (Van Nostrand Reinhold, New York, 1979)
13. K. Kirby, R.P. Saxon, B. Liu, Astrophys. J. **231**, 637 (1979)
14. L.-E. Berg, L. Klynning, Phys. Scripta **10**, 331 (1974)
15. P.F. Weck, P.C. Stancil, K. Kirby, J. Chem. Phys. **118**, 9997 (2003)
16. T. Leininger, G.-H. Jeung, J. Chem. Phys. **103**, 3942 (1995)
17. B. Barbuy, R.P. Schiavon, J. Gregorio-Hetem, P.D. Singh, C. Batalha, Astron. Astrophys. Suppl. Ser. **101**, 409 (1993)
18. M.V. Ramanaiah, S.V.J. Lakshman, Physica C **113**, 263 (1982)
19. O. Appelblad, L. Klynning, J.W.C. Johns, Phys. Scripta **33**, 415 (1986)
20. L.-E. Berg, K. Ekvall, A. Hishikawa, S. Kelly, C. McGuinness, Chem. Phys. Lett. **255**, 419 (1996)
21. P.W. Fairchild, G.P. Smith, D.R. Crosley, J.B. Jeffries, Chem. Phys. Lett. **107**, 181 (1984)
22. W.R. Anderson, D.R. Crosley, Chem. Phys. Lett. **62**, 275 (1979)
23. K.P. Kirby, E.M. Goldfield, J. Chem. Phys. **94**, 1271 (1991)
24. D.R. Yarkony, J. Chem. Phys. **91**, 4745 (1989)
25. J.W.C. Johns, F.A. Grimm, R.F. Porterm, J. Mol. Spectros. **22**, 435 (1967)
26. C.H. Douglass, H.H. Nelson, J.K. Rice, J. Chem. Phys. **90**, 6940 (1989)
27. J.K. Rice, L. Pasternack, H.H. Nelson, Chem. Phys. Lett. **189**, 43 (1992)
28. P. Baltayan, O. Nedelec, J. Chem. Phys. **70**, 2399 (1979)
29. S.R. Langhoff, C.W. Bauschlicher, Jr., J. Chem. Phys. **88**, 5715 (1988)
30. D.F. Rogowski, A. Fontijn, Chem. Phys. Lett. **137**, 219 (1987)
31. M. Larsson, Astron. Astrophys. **128**, 291 (1983)
32. J.H. Van Vleck, Astrophys. J. **80**, 161 (1934)
33. J.E. Littleton, S.P. Davis, Astrophys. J. **333**, 1026 (1988)
34. C.M. Olmsted, Astrophys. J. **27**, 66 (1908)
35. R.N. Zare, *Angular Momentum* (John Wiley and Sons, New York, 1988)
36. J. Flemming, A.M. Tuboy, D.M.B.P. Milori, L.G. Marcassa, S.C. Zilio, V.S. Bagnato, Opt. Comm. **135**, 269 (1997)
37. R. Gupta, C. Xie, S. Padua, H. Batelaan, H. Metcalf, Phys. Rev. Lett. **71**, 3087 (1993); Phys. Rev. Lett. **72**, 178(E) (1994)
38. E. Hirota, *High-Resolution Spectroscopy of Transient Molecules* (Springer, New York, 1985)
39. C.H. Townes, A.L. Schawlow, *Microwave Spectroscopy* (Dover, New York, 1975)
40. W.L. Barclay, Jr., M.A. Anderson, L.M. Ziurys, Astrophys J. **408**, L65 (1993)
41. C.I. Frum, J.J. Oh, E.A. Cohen, H.M. Pickett, Astrophys J. **408**, L61 (1993)
42. J.L. Féménias, Phys. Rev. A **15**, 1625 (1977)
43. E. Hulthèn, Phys. Rev. **29**, 97 (1927)
44. R. Pereira, S. Skowronek, A. González Ureña, A. Pardo, J.M.L. Poyatom, A.H. Pardo, J. Mol. Spec. **212**, 17 (2002)
45. T.C. Steimle, J. Gengler, J. Chen, Can. J. Chem. (to be published)
46. J. Weinstein, R. deCarvalho, T. Guillet, B. Freidrich, J.M. Doyle, Nature **395** 148 (1998)
47. B. Freidrich, J. Weinstein, R. deCarvalho, J.M. Doyle, J. Chem. Phys. **110**, 2376 (1999)
48. E.L. Raab, M. Prentiss, A. Cable, S. Chu, D.E. Pritchard, Phys. Rev. Lett. **59**, 2631 (1987)
49. H.E. Radford, Phys. Rev. **122**, 114 (1961)
50. J. Xina, I. Ionescub, D. Kuffelb, S.A. Reid, Chem. Phys. **291**, 61 (2003)
51. E.L. Hill, Phys. Rev. **34**, 1507 (1929)
52. M.D. Di Rosa, S.G. Crane, J.J. Kitten, W.A. Taylor, D.J. Vieira, X. Zhao, Appl. Phys. B **76**, 45 (2003).
53. K.E. Gibble, S. Kasapi, S. Chu, Opt. Lett. **17**, 526 (1992)
54. K. Lindquist, M. Stephens, C. Wieman, Phys. Rev. A **46**, 4082 (1992)
55. H.J. Davies, K. Szymaniec, C.S. Adams, Phys. Rev. A **62**, 013412 (2000)